Viscous and Elastic Perturbation Effects on Hypersonic Unsteady Airfoil Aerodynamics

Lars E. Ericsson*
Lockheed Missiles & Space Company, Inc., Sunnyvale, Calif.

In the present study a perturbation approach has been used to determine the dynamic effects of hypersonic viscid-inviscid interaction in laminar flow. It is shown that the experimentally observed changes of the inviscid unsteady aerodynamics of finite-thickness airfoils due to viscous effects and elastic deflection can be computed in a direct, simple manner using an embedded flow concept. Not only is the agreement good between present predictions and experimental static and dynamic data, the present perturbation method also gives results that are in close agreement with those obtained by use of numerical methods.

Nomenclature

a = speed of sound
B, B_1, B_2 = viscous parameters, Eq. (11)
c = chord length
C^* = Chapman-Rubesin parameter
G_1, G_2, G_e = parameters defined in Eqs. (13) and (32)
h = surface displacement (Fig. 11)
h_0 = airfoil camber (Fig. 12)
K = hypersonic similarity parameter [Eqs. (2, 3, and 45)]
M = Mach number, U/a
m_p = pitching moment for an airfoil strip: coefficient $c_m = m_p/(\rho_\infty U_\infty^2/2)c^2$
n = normal force for an airfoil strip: coefficient $c_n = n/(\rho_\infty U_\infty^2/2)c$
p = static pressure: coefficient $C_p = (p-p_\infty)/(\rho_\infty U_\infty^2/2)$
Pr = Prandtl number
q = rigid body pitch rate
R_b = radius of curvature (Fig. 12)
Re = Reynolds number, $Re_x = xU_e/\nu_e$ and $Re_{x\infty} = xU_\infty/\nu_\infty$
t = time
T = temperature
T^* = reference temperature
U = axial velocity
$V_\perp$ = velocity normal to surface
x = chord-wise coordinate (Fig. 1)
y_L, y_U = distance from chord centerline to lower and upper airfoil surface (Fig. 1)
y_b = cambered airfoil coordinate (Fig. 12)
α = angle of attack
α_0 = trim angle-of-attack
γ = ratio of specific heats ($\gamma = 1.4$ for air)
δ^* = boundary-layer displacement thickness
ϵ = density ratio across bow shock
θ = perturbation in pitch (Fig. 1)
θ_w = wedge half-angle
κ = dimensionless surface curvature, $\kappa = c/R_b\,\theta_w$
ν = kinematic viscosity of air
ξ = dimensionless x coordinate, $\xi = x/c$
ρ = air density
υ = surface inclination, $\upsilon = \tan^{-1}(\partial y/\partial x)$
$\bar{\chi}$ = viscous hypersonic similarity parameter, $\bar{\chi} = M_e^3\sqrt{C^*}/\sqrt{Re_x}$

Subscripts

A = aft body
b = body surface
c = centrifugal pressure correction
c.g. = center of gravity or oscillation center
d = deformation
e = boundary-layer edge
F = forebody
L = lower surface
i = inviscid flow
NB = Newtonian-Busemann value
γN = γ-corrected Newtonian value
PT = piston theory
t = total or stagnation value
TE = trailing edge
TW = tangent wedge
U = upper surface
v = viscosity effect
w = wall
o = initial value or constant parameter value
∞ = freestream conditions

Derivative Symbols

$\dot{\theta}$ = $\partial\theta/\partial t$
$c_{n\alpha}$ = $\partial c_n/\partial\alpha$; $c_{m\theta} = \partial c_m/\partial\theta$
c_{mq} = $\partial c_m/\partial(cq/U_\infty)$; $c_{m\dot{\alpha}} = \partial c_m/\partial(c\dot{\alpha}/U_\infty)$
$c_{m\dot{\theta}}$ = $c_{mq} + c_{m\dot{\alpha}}$
C_{pK} = $\partial C_p/\partial K$

Introduction

VISCOUS flow effects in low-density hypersonic flow have been investigated widely by both theoreticians and experimentalists. This is true at least in regard to static aerodynamics where the so-called viscid-inviscid interaction effects are well-established.[1] The dynamic effects of this hypersonic viscid-inviscid interaction have received much less attention, the only well-known work being that by Orlik-Rückemann et al.[2-5] In the present study, a simplified approach is used. The embedded flow concept used earlier to develop a simple analytic theory for computation of the effect of nose bluntness on slender vehicle unsteady aerodynamics[6,7] is pursued further in the present paper. It is shown that the experimentallly observed changes of the inviscid unsteady aerodynamics of finite-thickness airfoils due to viscous effects and elastic deflections can be computed in a direct, simple manner using the embedded flow concept. Not only is the agreement good between present predictions and experimental static and dynamic data, the present perturbation method also

Presented as Paper 77-5 at the AIAA 15th Aerospace Sciences Meeting, Los Angeles, Calif., Jan. 24-26, 1977; submitted Feb. 4, 1977; revision received May 25, 1977.

Index categories: Nonsteady Aerodynamics; Jets, Wakes, and Viscid-Inviscid Flow Interactions; Supersonic and Hypersonic Flow.

*Consulting Engineer. Associate Fellow AIAA.

gives results that are in close agreement with numerical results.[8-10]

Analysis

At hypersonic speeds the unsteady aerodynamics of an airfoil with sharp leading edge often is given with satisfactory accuracy by the simple piston theory for small flow inclination angles and by the Newtonian theory[11] for large flow deflections. The "tangent wedge" formulation,[11,12] which unifies these two theories, will be used to determine the inviscid characteristics. Thus, the pressure coefficient is defined as follows:

$$(C_p)_{TW} = \begin{cases} 0 & K \le -2/(\gamma-1) \\ \dfrac{2}{\gamma M_\infty^2}\left[\left(1+\dfrac{\gamma-1}{2}K\right)^{2\gamma/(\gamma-1)}-1\right] & -\dfrac{2}{\gamma-1} < K < 0 \\ \dfrac{2K}{M_\infty^2}\left[\dfrac{\gamma+1}{4}K+\sqrt{1+\left(\dfrac{\gamma+1}{4}K\right)^2}\right] & K \ge 0 \end{cases} \quad (1)$$

For a rigid airfoil describing oscillations of low reduced frequency $(c\omega/U_\infty)^2 \ll 1$, the hypersonic similarity parameter can be written

$$K = M_\infty V_\perp / U \quad (2)$$

where, from Fig. 1, $V_\perp/U$ is defined as follows for lower and upper surfaces:

$$\left(\frac{V_\perp}{U}\right)_L = \sin(\upsilon_L + \alpha_0 + \theta) + \frac{(x - x_{c.g.} + y_L \tan\upsilon_L)q}{U}\cos\upsilon_L \quad (3a)$$

$$\left(\frac{V_\perp}{U}\right)_U = \sin(\upsilon_U - \alpha_0 - \theta) - \frac{(x - x_{c.g.} + y_U \tan\upsilon_U)q}{U}\cos\upsilon_U \quad (3b)$$

$$\upsilon = \tan^{-1}(\partial y/\partial x) \quad (3c)$$

For $K \gg 1$, Eq. (1) gives

$$\lim_{K\to\infty}(C_p)_{TW} = (\gamma+1)M_\infty^{-2}K^2 \quad (4)$$

This agrees with the Newtonian value only for $\gamma = 1$. In order for the Newtonian theory to give the "correct" limit also for other γ values, the following gamma correction has to be made:

$$(C_p)_{\gamma N} = (\gamma+1)(V_\perp/U)^2 \quad (5)$$

This corresponds to the value $C_{ps} = \gamma + 1$ used in Ref. 13. For $K < 1$ series expansion of Eq. (1) gives the piston theory result.[14] For $K > 1$, Eq. (1) is equal to the so-called strong shock piston theory.[15]

The hypersonic similarity results in the preceding can be extended down to (low) supersonic Mach numbers by substituting the Prandtl-factor $\sqrt{M_\infty^2 - 1}$ for M_∞ in Eq. (2) for the definition of K.[11,16] The second-order thickness effects present at supersonic speeds disappear already at $M_\infty > 2$ according to numerical and experimental results.[17-20] The chordwise load distribution over the airfoil is in coefficient form

$$\partial c_n/\partial\xi = (C_p)_L - (C_p)_U \quad (6)$$

At $\alpha_0 = 0$ Eqs. (1-16) define the following derivatives at $\theta < \theta_w$ for a symmetric, sharp wedge ($\upsilon_L = \upsilon_U = \theta_w$)

$$\partial c_{n\theta}/\partial\xi = 2M_\infty C_{pK}\cos\theta_w \quad (7)$$

$$\partial c_{nq}/\partial\xi = 2M_\infty C_{pK}[\xi(1+\tan^2\theta_w) - \xi_{c.g.}]\cos\theta_w \quad (8)$$

For a thin wedge ($\tan^2\theta_w \ll 1$ and $\cos\theta_w \approx 1$), the following stability derivatives are obtained at $\alpha_0 = 0$

$$c_{n\theta} = 2M_\infty C_{pK} \quad (9a)$$

$$c_{m\theta} = -c_{n\theta}(1/2 - \xi_{c.g.}) \quad (9b)$$

$$c_{mq} = -c_{n\theta}[(1/2 - \xi_{c.g.})^2 + 1/12] \quad (9c)$$

For a double-wedge, diamond airfoil shape, the result at $\alpha_0 = 0$ is

$$c_{n\theta} = (c_{n\theta})_F + (c_{n\theta})_A = M_\infty(C_{pK} + C_{pK-}) \quad (10a)$$

$$c_{m\theta} = -(c_{n\theta})_F(1/4 - \xi_{c.g.}) - (c_{n\theta})_A(3/4 - \xi_{c.g.}) \quad (10b)$$

$$c_{mq} = -(c_{n\theta})_F[(1/4 - \xi_{c.g.})^2 + 1/48] - (c_{n\theta})_A[(3/4 - \xi_{c.g.})^2 + 1/48] \quad (10c)$$

where C_{pK-} is obtained from Eq. (1) with $K = -M_\infty\theta_w$ (or $-\theta_w\sqrt{M_\infty^2 - 1}$).

Equations (9) and (10) show that $M_\infty c_{n\theta}$, $M_\infty c_{m\theta}$, and $M_\infty c_{mq}$ are functions of K only. This is illustrated in Figs. 2a and 2b for single and double wedges, respectively. As expected, the tangent wedge values are well-represented by third-order piston theory for low K values, $K < 1$, and by the gamma-corrected Newtonian theory for high K values, $K > 1$. Orlik-Rückemann's experimental pitch damping data for a double wedge[4] fall well above the inviscid prediction (see Fig. 2b). The helium data point ($\gamma = 5/3$) has been corrected for γ effects using Eqs. (1) and (10). One feels inclined to agree with the authors that the observed 50% overshoot of inviscid predictions cannot be explained by pure boundary-layer effects,[2,3] but that some other effects, e.g., shock-wave/boundary-layer interaction at the trailing edge, must have caused it. One such mechanism has been demonstrated by Hulcher and Behrens.[21] They showed that at $\alpha = 15°$ the leeside laminar flow on a flat plate at $M_\infty = 6$ was separated from 70% chord to the trailing edge due to the wake recompression (shock). Thus, one can also expect the 9° double wedge to have a trailing edge separation (at $\alpha = 0$), especially in view of the higher Mach number. It has, in fact, been shown that a biconvex airfoil experiences laminar separated flow on the leeside aft half chord.[22] The loss of leeside expansion due to separation will generate a negative, statically destabilizing tail load. The dynamic effect will be stabilizing due to the convective time lag associated with this wake-induced separation,[23-25] and could easily cause the observed 50% increased damping. The method presented in Ref. 22 for prediction of the separation induced pressure increase at supersonic Mach numbers could possibly be applied also in the hypersonic speed region. Thus, with the information contained in Refs. 22-25 as a basis, analytical methods could be developed for prediction of the separated

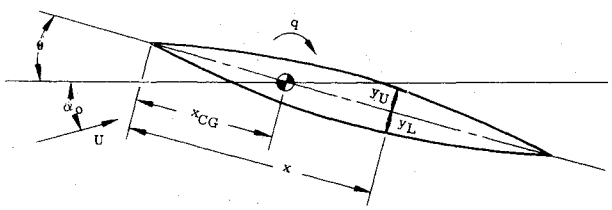

Fig. 1 Rigid airfoil pitch oscillations.

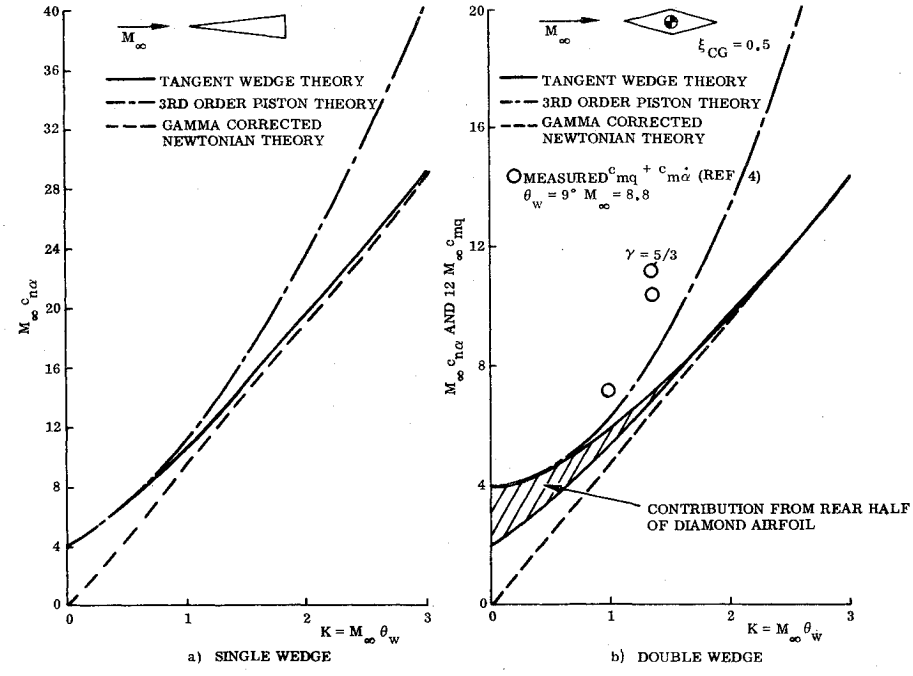

Fig. 2 Hypersonic aerodynamic derivatives.

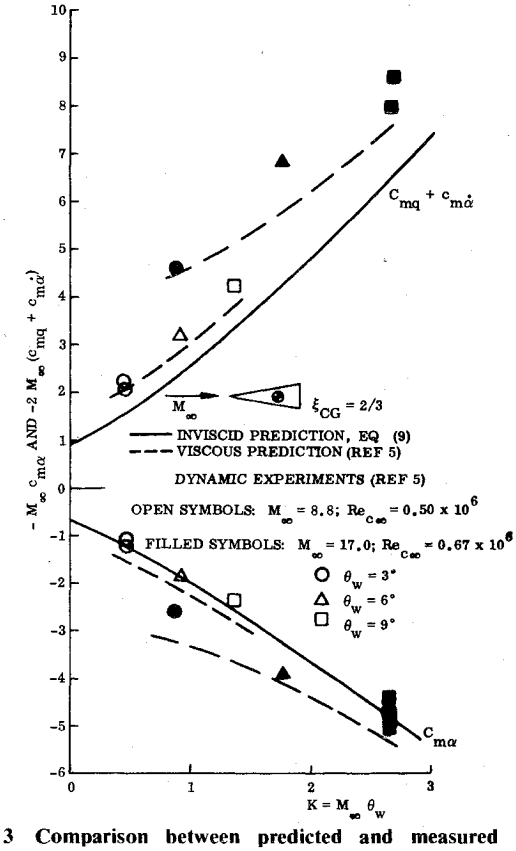

Fig. 3 Comparison between predicted and measured stability derivatives of a single wedge.

flow effect on the unsteady aerodynamic characteristics of double-wedge or lenticular shape airfoils. This is, however, beyond the scope of the present study.

For a single wedge, no trailing edge separation is present, and the deviations between inviscid predictions and preliminary experimental results[5] seem to be accounted for by the attached flow boundary-layer effect described by Orlik-Rückemann (see Fig. 3). However, one should be careful not to interpret the results as proof positive because of the inherent difficulties in performing a two-dimensional dynamic test, as the authors of Ref. 5 point out. The peculiar frequency effects observed in the test could well have been caused by wind-tunnel interference, as there is no known reason for the effects to be present in the free-flight case.

Viscous Flow Effects

The boundary layer on airfoils of vehicles travling at hypersonic speed will vary from being completely laminar at the high Mach number, high altitude end of the operating range to being mainly turbulent at low Mach numbers and altitudes. In regard to the boundary layer on the body, boundary-layer transition will play a role throughout the whole operating range, and will affect the unsteady aerodynamics significantly.[26] In the present study, however, only the laminar viscous effects on the two-dimensional unsteady airfoil aerodynamics will be considered.

The boundary-layer displacement surface increases the local inviscid flow angle by an amount $d\delta^*/dx$. The slope $d\delta^*/dx$ will be very small as compared to the angular changes of the inviscid flow, at least for the environment considered in the present study, and the effect of $d\delta^*/dx$ can be simulated by a small wedge embedded in the flow aft of the bow shock. Thus, the viscous perturbation effect is given, to first-order, by

$$\Delta p_v/p_e = \gamma K_v \qquad K_v = M_e d\delta^*/dx = B\bar{\chi} \tag{11a}$$

$$B = B_1 + B_2/M_e^2 \qquad \bar{\chi} = M_e^3\sqrt{C^*}/\sqrt{Re_x} \tag{11b}$$

$$Pr = 0.725 \quad B = 0.1445(\gamma - 1) + \left(0.9685\frac{T_w}{T_e} - 0.1035\right)\Big/M_e^2$$

$$= (\gamma - 1)\left[0.1445 + 0.4843\frac{T_w}{T_t}\right] + \left(0.9685\frac{T_w}{T_t} - 0.1035\right)\Big/M_e^2$$

$$Pr = 1 \quad B = 0.166(\gamma - 1) + 0.865\frac{T_w}{T_e}\Big/M_e^2$$

$$= (\gamma - 1)\left[0.166 + 0.4325\frac{T_w}{T_t}\right] + 0.865\frac{T_w}{T_t}\Big/M_e^2$$

According to Ref. 1, $C^* = 1$ for $T^* \leq 200°R$ and $C^* = (T^*/T_t)\{1 + [(\gamma - 1)/2]M_e^2\}^{-0.24}$ for reference temperatures in the range $200°F < T^* < 1000°R$, where $T^*/T_t = (1 + 3T_w/T_t)/6$.

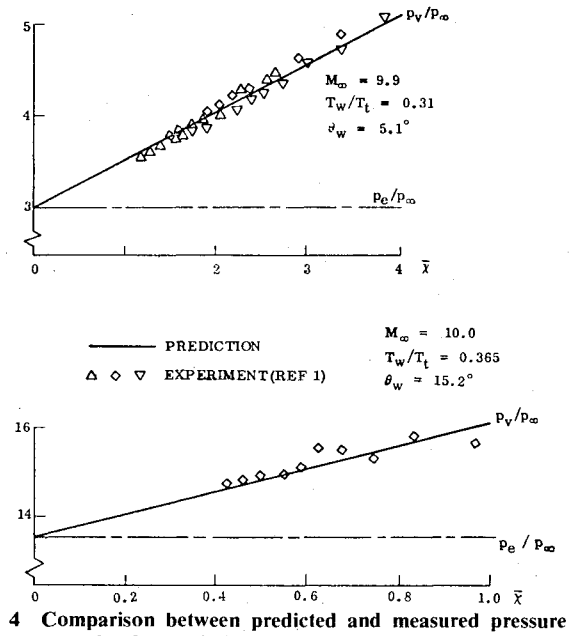

Fig. 4 Comparison between predicted and measured pressure increase on a wedge due to viscid-inviscid interaction.

For $M_e^2 \gg 1$, Eq. (11) simplifies to

$$\Delta p_v/p_e = \gamma B_1 \bar{\chi} \tag{12}$$

Predictions of $p_v/p_e = 1 + \Delta p_v/p_e$ using Eq. (12) agree well with experimental wedge data[1] for $M_\infty = 10$ (Fig. 4). The agreement persists up to large $\bar{\chi}$ values. However, when the wedge angle goes to zero, i.e., when all of the flow change is of viscous nature, Eq. (12) no longer predicts the measured pressures. In this case viscid-inviscid coupling effects must be included.[1,11] Nevertheless, on a finite chord airfoil trailing edge and separated flow effects often will dominate when these higher-order viscous effects should be considered; e.g., at $\alpha \neq 0$ for finite wedge angles ($\theta_w > 0$). Equation (11), or (12), for $M_e^2 \gg 1$, is especially convenient when using the local linearization approach in flutter analysis, as was done by Yates and Bennet.[13] As the self-induced pressure does not change the boundary-layer slope $d\delta^*/dx$ up to second-order accuracy,[11] the viscous induced effect on the surface pressure derivative is solely a function of inviscid flow parameters. The following simple result is obtained[27]:

$$\frac{d(\Delta C_{pv})/d\theta}{dC_{pe}/d\theta} = \frac{\Delta p_v}{p_e}\left\{\frac{5}{4} - \left(\frac{5}{4} - \frac{B_2}{BM_e^2}\right)G_1 - G_2\right\} \tag{13}$$

$$G_1 = \frac{1+\frac{\gamma-1}{2}M_\infty^2}{\frac{\gamma+1}{2}M_e^2} \frac{\left(\frac{p_e}{p_\infty}\right)^2 + 2\frac{\gamma-1}{\gamma+1}\left(\frac{p_e}{p_\infty}\right)+1}{\left(\frac{p_e}{p_\infty}\right)\left[1+\frac{\gamma-1}{\gamma+1}\left(\frac{p_e}{p_\infty}\right)\right]^2} \tag{13a}$$

$$G_2 = \frac{3\gamma}{(\gamma+1)^2} \frac{p_e/p_\infty}{\left[\left(\frac{p_e}{p_\infty}\right)+\frac{\gamma-1}{\gamma+1}\right]\left[1+\frac{\gamma-1}{\gamma+1}\left(\frac{p_e}{p_\infty}\right)\right]} \tag{13b}$$

$$M_e^2 = \frac{M_\infty^2\left[(\gamma+1)\left(\frac{p_e}{p_\infty}\right)+(\gamma-1)\right]-2\left[\left(\frac{p_e}{p_\infty}\right)^2-1\right]}{(\gamma+1)\left(\frac{p_e}{p_\infty}\right)\left[1+\frac{\gamma-1}{\gamma+1}\left(\frac{p_e}{p_\infty}\right)\right]} \tag{13c}$$

$\Delta p_v/p_e$ and $B = B_1 + B_2/M_e^2$ are defined in Eq. (11), and $p_e/p_\infty = 1 + (\gamma/2)\,M_\infty^2\,C_p$ is given by Eq. (1), substituting $K\sqrt{1-M_\infty^{-2}}$ for K at lower Mach numbers.[16]

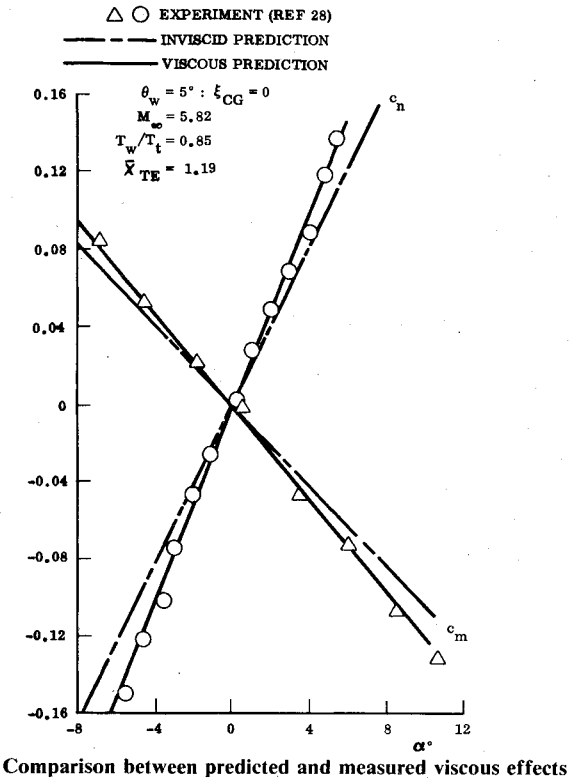

Fig. 5 Comparison between predicted and measured viscous effects on the aerodynamic characteristics of a 5° wedge.

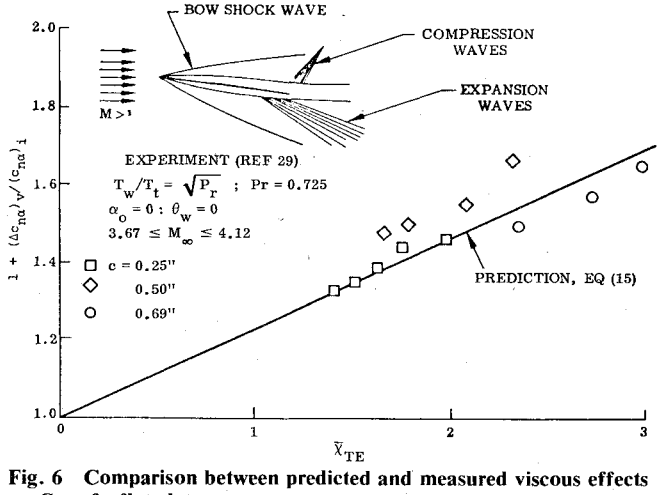

Fig. 6 Comparison between predicted and measured viscous effects on $C_{n\alpha}$ of a flat plate.

The relative change of inviscid aerodynamic derivatives due to viscous first-order perturbation effects can be obtained for arbitrary thin airfoils using Eq. (13). For a wedge the result becomes particularly simple, as $M_e = \text{const}$ and $\bar{\chi} = \bar{\chi}_{TE}\,\xi^{-1/2}$. Integration of Eq. (13) then gives, for upper and lower surfaces, the following relationship:

$$\frac{(\Delta c_{n\theta})_v}{(C_{p\theta})_e} = 2\left[\frac{d(\Delta C_{pv})/d\theta}{d(C_{pe})/d\theta}\right]_{TE}; \quad \frac{(\Delta c_{m\theta})_v}{(\Delta c_{n\theta})_v} = -\left(\frac{1}{3} - \xi_{c.g.}\right) \tag{14}$$

Noticing that $(C_{p\theta})_e = (\Delta c_{n\theta})_i$, Eq. (14) gives the viscous induced increment of upper and lower surface inviscid aerodynamic derivatives. At $\alpha = 0$, it gives the total result for both surfaces, that is,

$$\frac{(\Delta c_{n\theta})_v}{(c_{n\theta})_i} = 2\left[\frac{d(\Delta C_{pv})/d\theta}{d(C_{pe})/d\theta}\right]_{TE} \tag{15}$$

Within the linear α range, Eq. (15) also expresses the ratio $\Delta c_{nv}/c_{ni}$. In Figs. 5 and 6, predictions through Eq. (15) are

compared with available experimental data.[28,29] The good agreement for the 5° wedge (Fig. 5) was expected, but the good agreement with the flat-plate data (Fig. 6) was a surprise in view of the failure of Eq. (12) to predict Sliski's flat-plate data.[1] The experimental data were underpredicted by 30%. This also may be the lift loss of a finite chord flat plate due to the trailing edge effect discussed by the authors of Ref. 29 (see inset in Fig. 6). Thus, fortuitously, Eq. (15) will give the correct viscous effect on the lift even for the limiting case when $\theta_w \to 0$. However, the moment contribution will not be predicted as well, and neither will the viscous effect on unsteady aerodynamics. Nevertheless, as was discussed before, a very accurate prediction of the pure viscous interaction for zero inviscid flow inclination to the surface is not essential for prediction of the airfoil aerodynamics. Judging by the good agreement between predicted and measured viscous influence on the moment of the 5° wedge (Fig. 5), this trailing edge effect is small even for respectable values ($\bar{\chi}_{TE} = 1.3$) of the hypersonic viscous similarity parameter. As this parameter $\bar{\chi}_{TE}$ is increased, the strong interaction region near the leading edge and the near wake effect at the trailing edge both become more important. For finite base height, e.g., for $\theta_w > 0$, the wake recompression effects are fed upstream through the near wake, adding complexity to the trailing edge effect.[24,25]

Equations (14) and (15) define the following viscous-induced forward shift of the aerodynamic center:

$$(\Delta\xi_{AC})_v = -\frac{1}{6}\frac{(\Delta c_{n\theta})_v}{(c_{n\theta})_i}\left[1+\frac{(\Delta c_{n\theta})_v}{(c_{n\theta})_i}\right] \tag{16}$$

Unsteady Aerodynamics

The change of effective airfoil geometry produced by the boundary-layer displacement surface and the corresponding effect on static stability derivatives were considered in the previous section. There is, of course, a similar effect on the dynamic stability derivative. Equation (13) defines the following strip load derivative distribution:

$$\frac{\mathrm{d}(\Delta c_{n\theta})_v}{\mathrm{d}\xi} = \left[\frac{\mathrm{d}(\Delta C_{pv})}{\mathrm{d}\theta}\right]_L - \left[\frac{\mathrm{d}(\Delta C_{pv})}{\mathrm{d}\theta}\right]_U \tag{17}$$

And the running load increment due to viscous wedge thickening is

$$\frac{\mathrm{d}(\Delta c_n)_v}{\mathrm{d}\xi} = \frac{\mathrm{d}(\Delta c_{n\theta})_v}{\mathrm{d}\xi}\frac{V_\perp}{U_\infty} \tag{18}$$

For a wedge describing rigid body oscillations in pitch around $x = x_{\mathrm{c.g.}}$, Eqs. (3, 13, 17, and 18) give, for $\alpha_0 = 0$

$$\frac{\mathrm{d}(\Delta c_{nq})_v}{\mathrm{d}\xi} = 2\left[\frac{\mathrm{d}(\Delta C_{pv})}{\mathrm{d}\theta}\right]_{TE}\xi^{-1/2}(\xi - \xi_{\mathrm{c.g.}}) \tag{19}$$

Integrating Eq. (19) and its moment contribution gives

$$\Delta(c_{nq})_v = -\Delta(c_{m\theta})_v = \Delta(c_{n\theta})_v(\tfrac{1}{3} - \xi_{\mathrm{c.g.}}) \tag{20}$$

$$\Delta(c_{mq})_v = -\Delta(c_{n\theta})_v[4/45 + (\tfrac{1}{3} - \xi_{\mathrm{c.g.}})^2] \tag{21}$$

The ratio $\Delta(c_{N\theta})_v/(c_{n\theta})_i$ is given by Eqs. (13-15), as was discussed earlier. Equation (21) shows that the viscous induced thickening of the wedge increases the aerodynamic damping, the effect being smallest for $\xi_{\mathrm{c.g.}} = \frac{1}{3}$. Orlik-Rückemann has shown that, in addition to this static interaction, it is important to consider the "dynamic interaction," resulting from the fact that the boundary-layer displacement thickness does not remain constant during the oscillation.[8] The boundary layer becomes thinner on the windward side. On the oscillating airfoil, this boundary-layer "cushioning" decreases the "piston effectiveness" by changing the inviscid velocity ratio $(V_\perp/U_e)_i$ by an amount $(\mathrm{d}\delta^*/\mathrm{d}t)/U_e$. This local reaction can be assumed to occur instantaneously for the structural and rigid body frequencies of practical interest. At large $\bar{\chi}_{TE}$, one may have to consider downstream effects of changes occurring at an earlier time instant in the strong interaction region near the leading edge, as well as upstream effects of changes in the near wake recirculatory flow (also occurring at an earlier time instant). These effects are not considered in the present analysis.

For most applications it can be assumed that the missile velocity changes slowly as compared to structural and rigid body frequencies. Thus, the time derivative $\mathrm{d}\xi^*/\mathrm{d}t$ is solely the result of the perturbations of the relative piston velocity $V_\perp/U_\infty$, defined by Eq. (3); that is

$$\frac{\mathrm{d}\delta^*}{\mathrm{d}t} = \frac{\partial\delta^*}{\partial\theta}\frac{\mathrm{d}}{\mathrm{d}t}\left(\frac{V_\perp}{U_\infty}\right) \tag{22}$$

Whereas the boundary-layer slope $\mathrm{d}\delta^*/\mathrm{d}x$ is relatively insensitive to the ambient pressure gradient, the boundary-layer thickness itself is not, but it becomes thinner for increasing pressures.[11] Bertram et al.[30] have shown that this fact can be represented by assuming the boundary-layer thickness to be inversely proportional to $\sqrt{p_v/p_\infty}$. In the perturbation approach used here, p_v/p_∞ is in the first iteration represented by the inviscid pressure ratio p_e/p_∞. Thus, δ^* is modified as follows:

$$\frac{\mathrm{d}\delta^*}{\mathrm{d}x} = \frac{\delta^*}{2x} = \left(\frac{\mathrm{d}\delta^*}{\mathrm{d}x}\right)_{FP}\Big/\sqrt{\frac{p_e}{p_\infty}} \tag{23}$$

When $p_e/p_\infty \to 1$ the flat plate value is recovered. From Eqs. (11, 13, and 23) is obtained

$$\frac{1}{x}\frac{\mathrm{d}\delta^*}{\mathrm{d}\theta} = -\frac{\mathrm{d}C_{pe}}{\mathrm{d}\theta}\frac{\Delta p_v}{p_e}\left(\frac{p_e}{p_\infty}\right)^{-3/2}\frac{M_\infty^2}{M_e}\left\{\frac{3}{4} - \frac{B_2}{BM_e^2}G_1 + G_2 + \frac{1}{4}\right\} \tag{24}$$

The change of piston effectiveness $\dot{\delta}^*/U_e$ can be written

$$\frac{\dot{\delta}^*}{U_e} = \frac{\dot{\delta}^*}{U_\infty}\frac{U_\infty}{U_e} = \frac{\dot{\theta}c}{U_\infty}\xi\frac{M_\infty}{M_e} \times\left[\frac{1+[(\gamma-1)/2]M_e^2}{1+[(\gamma-1)/2]M_\infty^2}\right]^{1/2}\left(\frac{1}{x}\frac{\mathrm{d}\delta^*}{\mathrm{d}\theta}\right) \tag{25}$$

Again, using the embedded formulation, Eq. (11) gives

$$\Delta p_v(\dot{\delta}^*)/p_e = \gamma M_e\dot{\delta}/U_e \tag{26}$$

Combining Eqs. (23-25) finally gives

$$\frac{\mathrm{d}\Delta C_{pv}(\dot{\delta}^*)}{\mathrm{d}(c\dot{\theta}/U_\infty)} = -2\xi\frac{\Delta p_v}{p_e}\left(\frac{p_e}{p_\infty}\right)^{1/2}\frac{M_\infty}{M_e} \times\left[\frac{1+[(\gamma-1)/2]M_e^2}{1+[(\gamma-1)/2]M_\infty^2}\right]^{1/2}\left\{\frac{3}{4} - \frac{B_2}{BM_e^2}G_1 + G_2 + \frac{1}{4}\right\} \tag{27}$$

In general, M_e and $\Delta p_v/p_e$ are functions of ξ. However, for a wedge, Eq. (27) simplifies to

$$\frac{\mathrm{d}[\Delta C_{pv}(\dot{\delta}^*)]}{\mathrm{d}(c\dot{\theta}/U_\infty)} = \xi^{1/2}\frac{\mathrm{d}[\Delta C_{pv}(\dot{\delta}^*)]_{TE}}{\mathrm{d}(c\dot{\theta}/U_\infty)} \tag{28}$$

Integrating Eq. (28) gives the following result for pitch oscillations around $x = x_{\mathrm{c.g.}}$ at $\alpha = 0$:

$$(\Delta c_{n\dot{\alpha}})_v = \frac{\mathrm{d}[\Delta c_{nv}(\dot{\delta}^*)]}{\mathrm{d}(c\dot{\theta}/U_\infty)} = \frac{4}{3}\frac{\mathrm{d}[\Delta C_p(\dot{\delta}^*)]_{TE}}{\mathrm{d}(c\dot{\theta}/U_\infty)} \tag{29a}$$

$$(\Delta c_{m\dot{\alpha}})_v = -(\Delta c_{n\dot{\theta}})_v(3/5 - \xi_{\mathrm{c.g.}}) \tag{29b}$$

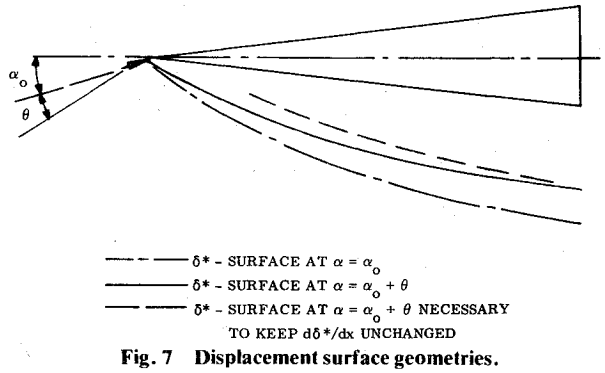

Fig. 7 Displacement surface geometries.

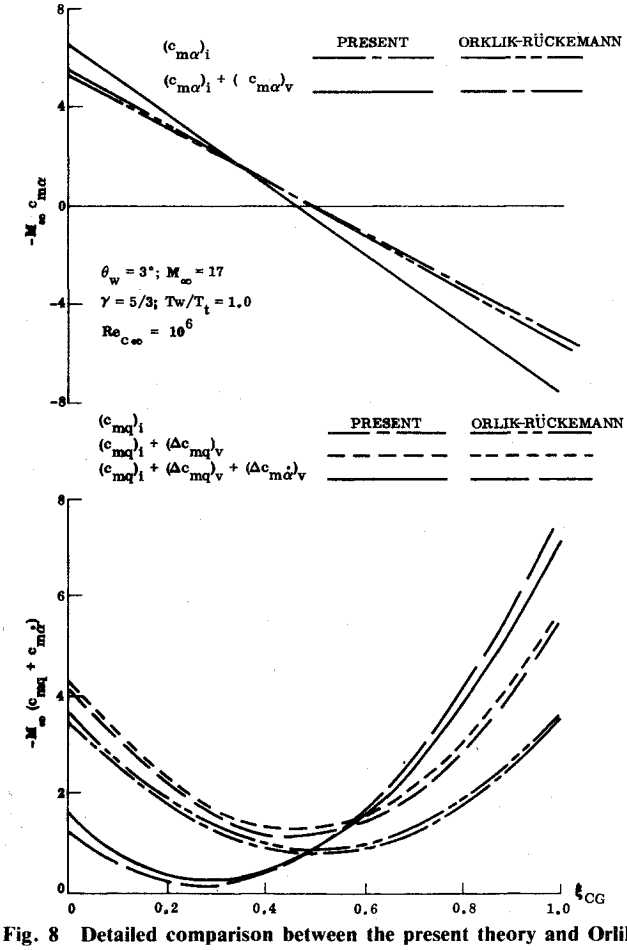

Fig. 8 Detailed comparison between the present theory and Orlik-Rückemann's theory.

$$\frac{d[\Delta C_p(\dot{\delta}^*)]_{TE}}{d(c\dot{\theta}/U_\infty)} = -\left(\frac{\Delta p_v}{p_e}\right)_{TE} \frac{(c_{n\theta})_i}{\sqrt{p_e/p_\infty}} \frac{M_\infty}{M_e}$$

$$\times \sqrt{\frac{1+[(\gamma-1)/2]M_e^2}{1+[(\gamma-1)/2]M_\infty^2}} \left\{\left(\frac{3}{4} - \frac{B_2}{BM_e^2}\right) G_1 + G_2 + \frac{1}{4}\right\} \quad (29c)$$

Combining Eqs. (13-15, 21, and 29) with Eq. (9) gives the damping ratios

$$\frac{(\Delta c_{mq})_v}{c_{mq}} \Big/ \frac{(\Delta c_{n\theta})_v}{(c_{n\theta})_i} = \frac{[(\frac{1}{3} - \xi_{c.g.})^2 + 4/45]}{[(\frac{1}{2} - \xi_{c.g.})^2 + 1/12]} \quad (30)$$

$$\frac{(\Delta c_{m\dot{\alpha}})_v}{c_{mq}} \Big/ \frac{(\Delta c_{n\theta})_v}{(c_{n\theta})_i} = -G_e\left(\frac{3}{5} - \xi_{c.g.}\right) \Big/ \left[\left(\frac{1}{2} - \xi_{c.g.}\right)^2 + \frac{1}{12}\right] \quad (31)$$

$$G_{eo} = \frac{2}{3}\left(\frac{p_e}{p_\infty}\right)^{-1/2} \frac{M_\infty}{M_e} \left(\frac{1+\frac{\gamma-1}{2}M_e^2}{1+\frac{\gamma-1}{2}M_\infty^2}\right)^{1/2}$$

$$\times \frac{\left(\frac{3}{4} - \frac{B_2}{BM_e^2}\right)G_1 + G_2 + \frac{1}{4}}{\frac{5}{4} - \left(\frac{5}{4} - \frac{B_2}{BM_e^2}\right)G_1 - G_2} \quad (32)$$

G_{eo} is the zero-order estimate, valid when $\Delta p_v/p_e \ll 1$. In order to obtain a better estimate, one must account, in some manner, for the fact that $p_v \neq p_e$, and for the presence of the self-induced pressure gradient.[11] Figure 7 illustrates the windward side displacement surface for different cases. Equation (23), with p_e substituted by p_v, assumes the displacement surface perturbation illustrated by the dashed line in Fig. 7. In order to account for the effect of the $(\Delta p_v/p_e)-$ distribution along the surface on the displacement thickness δ^*, one would try to find a point somewhere near mid-chord ($\xi^* \approx 0.5$) which could represent the integrated effect in lumped form by the local value of $\Delta p_v/p_e$ at $\xi = \xi^*$. In reality, the δ^* surface does not describe a pure translation, but does also rotate, as is illustrated by the solid line in Fig. 7. Thus, the chord-wise station representing, in lumped form, the effect of the $(\Delta p_v/p_e)$ distribution must be closer to the trailing edge, i.e., $0.5 < \xi^* \leq 1.0$. The trailing edge is the obvious choice for the next estimate, the first-order estimate of G_e. Thus, G_{el} is obtained from Eq. (32) by replacing p_e by $p_v = [1 + \Delta p_v/p_e]p_e$.

In Fig. 8, the results of the present perturbation analysis, Eqs. (15-17) and (29-32), are compared with those of Orlik-Rückemann's more exact numerical analysis.[8] The agreement is excellent between the two theories, and both theories are in good agreement with experimental results[5] (Fig. 9).

Nonviscous Applications

The perturbation analysis performed for viscous flow can be applied easily to other surface perturbations, e.g., those caused by elastic deflections. Mandl[9,10] has investigated numerically the effect of one particular type of surface deformation (see inset in Fig. 10). In this case, the following equivalence holds:

$$d\xi^*/dx = \kappa\theta_w\xi \quad (33)$$

where $\kappa = c/R\ \theta_w$; $\kappa^2 \ll 1$. $\kappa > 0$ for concave, and $\kappa < 0$ for convex surface deformation. Again using the embedded flow approach, the equation corresponding to Eq. (11), giving the deformation-induced relative pressure increase, is

$$\Delta p_d/p_e = \gamma M_e \kappa\ \theta_w \xi \quad (34)$$

and the following equation corresponding to Eq. (13) is obtained:

$$\frac{d(\Delta C_{pd})/d\theta}{d(C_{pe})/d\theta} = (\Delta p_d/p_e)(1 - G_1/2) \quad (35)$$

The equation corresponding to Eqs. (14) and (15) is

$$\frac{(\Delta c_{n\theta})_d}{(c_{n\theta})_i} = \frac{1}{2}\left[\frac{d(\Delta C_{pd})/d\theta}{d(C_{pe})/d\theta}\right]_{TE}; \quad \frac{(\Delta c_{m\theta})_d}{(\Delta c_{n\theta})_d} = -\left(\frac{2}{3} - \xi_{c.g.}\right) \quad (36)$$

The effect on the dynamic derivatives is obtained equally simply, the equation corresponding to Eq. (19) being

$$d(c_{nq})_d/d\xi = 2[d(\Delta c_{pd})/d\theta]_{TE}\xi(\xi - \xi_{c.g.}) \quad (37)$$

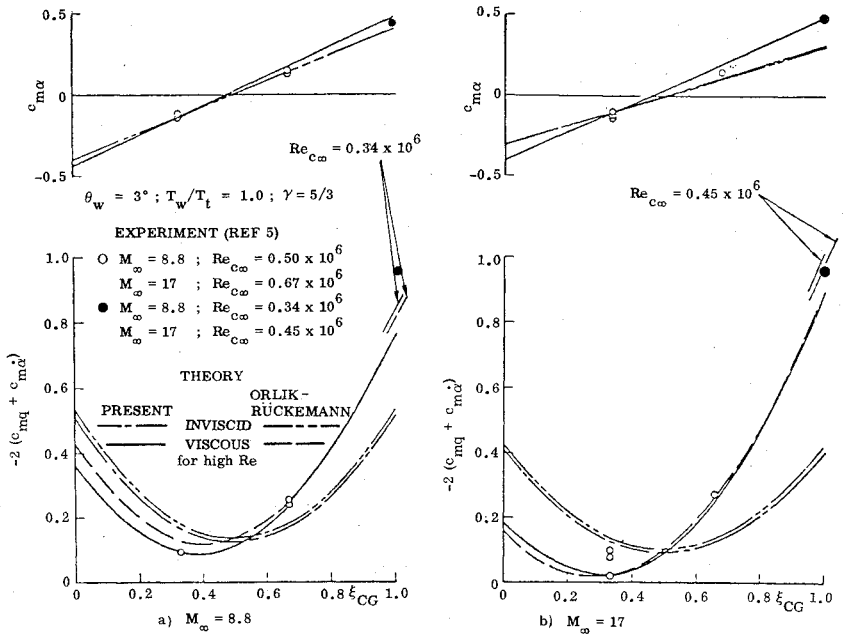

Fig. 9 Comparison between predicted and measured viscous effects on static and dynamic stability derivatives of a 3° wedge for heated wall conditions.

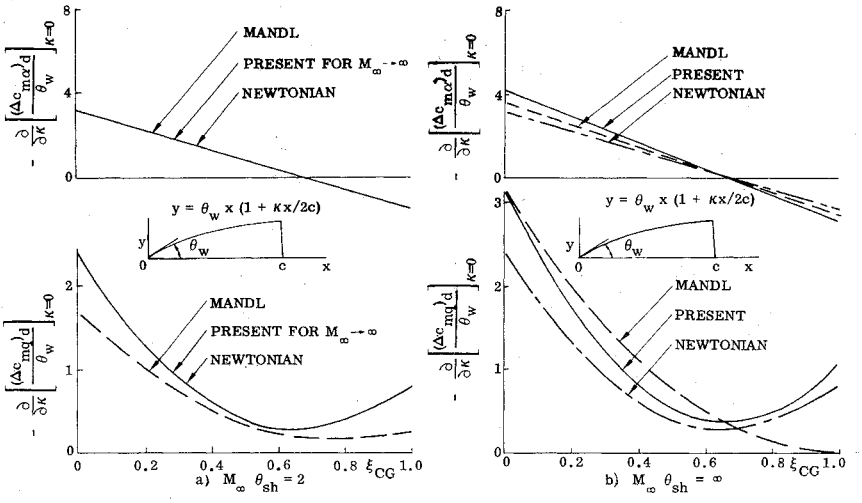

Fig. 10 Comparison of present elastic perturbation results with other theories.

which, after integration, gives

$$(\Delta c_{nq})_d = -(\Delta c_{m\theta})_d = (\Delta c_{n\theta})_d(\tfrac{2}{3} - \xi_{c.g.}) \tag{38}$$

$$(\Delta c_{mq})_d = -(\Delta c_{n\theta})_d[(\tfrac{2}{3} - \xi_{c.g.})^2 + 1/18] \tag{39}$$

As there is no "piston cushioning" in this case, $(\Delta c_{n\dot{\alpha}})_d = (\Delta c_{m\dot{\alpha}})_d = 0$, and the total effect on damping is the C_{mq} change. Thus, Eqs. (9) and (39) give

$$\frac{(\Delta c_{mq})_d}{(c_{mq})_i} \Big/ \frac{(\Delta c_{n\theta})_d}{(c_{n\theta})_i} = -\left[\left(\frac{2}{3} - \xi_{c.g.}\right)^2 + \frac{1}{18}\right] \Big/ \left[\left(\frac{1}{2} - \xi_{c.g.}\right)^2 + \frac{1}{12}\right] \tag{40}$$

Instead of moving the aerodynamic center forward, as in the viscous case [Eq. (16)] an equally large aft moment is obtained:

$$(\Delta\xi_{AC})_d = \frac{1}{6}\frac{(\Delta c_{n\theta})_d}{(c_{n\theta})_i} \Big/ \left[1 + \frac{(\Delta c_{n\theta})_d}{(c_{n\theta})_i}\right] \tag{41}$$

In Fig. 10 the κ derivatives obtained from Eqs. (13) and (34-41) are compared with Mandl's numerical results.[9,10] The agreement is satisfactory for axis locations of interest, $\xi_{c.g.} < 0.75$, and indicates that the present perturbation method is sufficiently accurate for the small elastic deformation considered in most elastic analyses.

Centrifugal Pressure Correction

When the surface has a longitudinal curvature, the pressure formulas derived earlier have to be corrected for the curvature effect.[11] With Busemann's centrifugal pressure correction included, the Newtonian pressure is

$$(p/p_\infty)_{NB} = 1 + \gamma K^2/(1-\epsilon) - \gamma M_\infty^2 y_b(x)/R_b(x) \tag{42}$$

ϵ is the density ratio through the (bow) shock and $R_b(x)$ is the (longitudinal) radius of curvature. For the present analysis of thin airfoils, $(1-\epsilon) \approx 2/(\gamma+1)$ and $1/R_b(x) \approx -\partial^2 y_b / \partial x^2$. From Fig. 1 is obtained

$$(y_b)_{\substack{L \\ U}} = h(x) - h(0) \pm (y)_{\substack{L \\ U}} \tag{43}$$

For a thin airfoil, the pressure coefficient given by Eq. (42) is

$$(C_p)_{NB} = (C_p)_{\gamma N} + (\Delta C_p)_c \tag{44a}$$

$$(C_p)_{\gamma N} = (\gamma+1)(V_\perp/U)^2 \tag{44b}$$

$$(\Delta C_p)_c = -2y_{yb}/R_b \approx 2y_b \partial^2 y_b/\partial x^2 \tag{44c}$$

In the case of the elastically deforming airfoil, Eq. (3) becomes

$$\left(\frac{V_\perp}{U}\right)_L = \sin\left(v_L + \alpha_0 + \frac{\partial h}{\partial x}\right) + \frac{1}{U}\frac{\partial h}{\partial t}\cos v_L \tag{45a}$$

$$\left(\frac{V_\perp}{U}\right)_U = \sin\left(v_U - \alpha_0 - \frac{\partial h}{\partial x}\right) - \frac{1}{U}\frac{\partial h}{\partial t}\cos v_U \tag{45b}$$

h is the centerline displacement normal to the rigid wing chord (see Fig. 11). In a general aeroelastic analysis, the deflection h is the sum of the deformations in a large number of elastic degrees of freedom.

Effect of Airfoil Camber

An infinitely thin airfoil with circular arc camber is sketched in Fig. 12. The following relationships between geometric parameters hold for $(h_0/R_b)^2 \ll 1$:

$$\frac{h_0}{R_b} = \frac{1}{2}\left(\frac{x}{R_b}\right)^2;\ \frac{h_0}{x} = \frac{1}{2}\frac{x}{R_b};\ v(x) - v(0) = \frac{x}{R_b} = 2\frac{h_0}{x} \tag{46}$$

According to Newtonian theory, only the windward side has a nonzero pressure coefficient. For a small angle of attack, Eq. (43) becomes

$$(y_b)_L = h_0 + x\alpha \tag{47}$$

And Eq. (35) gives

$$(C_p)_{\gamma N} = (\gamma+1)\left[\left(\frac{x}{R_b}\right)+\alpha\right]^2;\ \Delta C_{pc} = \left(\frac{x}{R_b}\right)^2 + \frac{2\alpha x}{R_b} \tag{48}$$

The α derivative is

$$\frac{\partial (C_p)_{\gamma N}}{\partial \alpha} = 2(\gamma+1)\left[\frac{x}{R_b}+\alpha\right] \quad \frac{\partial(\Delta C_{pc})}{\partial \alpha} = 2\frac{x}{R_b} \tag{49}$$

Finally, the effect of camber on the α derivative at $\alpha = 0$ is

$$\frac{\partial[\partial (C_p)_{\gamma N}/\partial\alpha]}{\partial (h_0/x)} = 4(\gamma+1);\quad \frac{\partial[\partial(\Delta C_{pc})/\partial\alpha]}{\partial(h_0/x)} = 4 \tag{50}$$

Thus, the centrifugal pressure correction increases the Newtonian pressure curvature derivatives by the factor $[1+(\gamma+1)^{-1}]$. In the case of the pure Newtonian theory, $\gamma+1=2$, and Busemann's correction increases the Newtonian pressure by 50% (see Ref. 11).

Effect of Surface Curvature

If one turns Fig. 12 around 180° and reverses the freestream flow direction, the figure can represent the windward side of a circular arc (bicusped) airfoil. In that case, Eqs. (48-50) will represent the pressure derivatives if the sign for the $(\Delta C_p)_c$ term is reversed. That is, the strip normal force derivative, $dc_{n\alpha}/d\xi$, is decreased by the ratio $1-(1+\gamma)^{-1}$ from the Newtonian value. Note that $2h_0/x$ represents the change in surface slope between the leading edge and station x [see Eq. (46)]. Mandl[9,10] investigated the effect of constant surface curvature on the aerodynamic characteristics of a wedge-shaped airfoil (see inset in Fig. 10 for a definition of the geometry). In this case, Eqs. (48-50) become (for the windward side)

$$(C_p)_{\gamma N} = (\gamma+1)[\theta_w(1+\kappa\xi)+\alpha]^2 \tag{51a}$$

$$(\Delta C_p)_c = 2\kappa\theta_w\xi[\theta_w(1+\kappa/2\xi)+\alpha] \tag{51b}$$

$$(\partial C_p/\partial\alpha)_{\gamma N} = 2(\gamma+1)[\theta_w(1+\kappa\xi)+\alpha] \tag{52a}$$

$$\partial(\Delta C_{pc})/\partial\alpha = 2\kappa\theta_w\xi \tag{52b}$$

For $\alpha = 0$

$$\partial[\partial C_p/\partial\alpha]_{\gamma N}/\partial\kappa = 2(\gamma+1)\theta_w\xi \tag{53a}$$

$$\partial[\partial(\Delta C_{pc})/\partial\alpha]/\partial\kappa = 2\theta_w\xi \tag{53b}$$

Again, the derivatives at $\alpha = 0$ are increased by the factor $[1+(\gamma+1)^{-1}]$ above the Newtonian value because of concave curvature effect. Convex curvature has, of course, the opposite effect, the factor then being $[1-(\gamma+1)^{-1}]$. For the standard Newtonian theory with Busemann's centrifugal correction, Eq. (53) becomes[11]:

$$\partial[\partial C_p/\partial\alpha]_N/\partial\kappa = 4\theta_w\xi \tag{54a}$$

$$\partial[\partial(\Delta C_{pc})/\partial\alpha]_B/\partial\kappa = 2\theta_w\xi \tag{54b}$$

That is, the centrifugal pressure correction increases the Newtonian value by 50%. It is shown in Ref. 31 that the viscous-induced curvature effect is negligibly small.

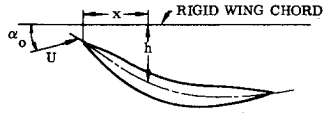

Fig. 11 Elastic airfoil oscillations.

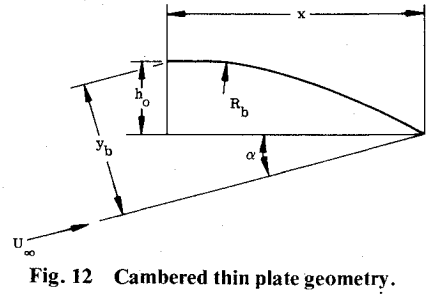

Fig. 12 Cambered thin plate geometry.

Elastic Perturbations

For a thin, symmetric airfoil, the elastic deflection is represented by the deformation of the centerchord line (see Fig. 11). In this case, the following equivalence with the viscous analysis is obtained

$$d\xi^*/dx = dh/dx \tag{55}$$

The deformation-induced relative pressure increase, given by Eq. (11), is

$$(\Delta p_E/p_e)_{\substack{L\\U}} = \pm\gamma M_e dh/dx \tag{56}$$

To this should be added the curvature effect from Eq. (44); that is,

$$[(\Delta C_{pE})_c]_{\substack{L\\U}} = \pm 2(y_b)_{\substack{L\\U}} d^2h/dx^2 \tag{57}$$

where $(y_b)_{\substack{L\\U}}$ is defined by Eq. (44). For a wedge describing parabolic elastic deformations, one can write $h(x)$ as follows:

$$dh/dx = \alpha + \bar{\kappa}\theta_w\xi;\quad h/c = h(0)/c + (\bar{\kappa}\theta_w/2)\xi^2 \tag{58}$$

The equations corresponding to Eqs. (56) and (57) become

$$(\Delta p_E/p_e)_L = \gamma M_e(\alpha + \bar{\kappa}\theta_w\xi) \tag{59a}$$

$$[(\Delta C_{pE})_c]_L = 2\bar{\kappa}\theta_w[\alpha\xi + (\bar{\kappa}\theta_w/2)\xi^2] \tag{59b}$$

The $\bar{\kappa}$ derivatives are in angular measure

$$\partial(\Delta C_{pE})_c/\partial(\bar{\kappa}\theta_w\xi) = 2(p_e/p_\infty)/(M_e/M_\infty^2) \tag{60a}$$

$$\partial(\Delta C_{pE})_c/\partial(\bar{\kappa}\theta_w\xi) = 2(\alpha+\theta_w\bar{\kappa}\xi) \tag{60b}$$

That is, for $\alpha=0$ and $\bar{\kappa}\to 0$, the centrifugal pressure correction goes to zero.

Surface Curvature Perturbations

For a wedge with a parabolic surface curvature superimposed (see inset in Fig. 10) the κ-derivative defined by Eqs. (34) and (35) is

$$(\partial/\partial\kappa)[(\Delta C_{pc})/\partial\theta] = (\partial C_{pe}/\partial\theta)\gamma M_e\theta_w\xi(1-G_1/2) \tag{61}$$

To this should be added the centrifugal pressure correction from Eq. (52) or Eq. (53). For $\alpha=0$, one obtains

$$\frac{\partial}{\partial\kappa}\left[\frac{\partial(\Delta C_{pd})}{\partial\theta}+\frac{\partial(\Delta C_{pc})}{\partial\theta}\right] = \frac{\gamma(\gamma+2)}{\gamma+1}\left(1-\frac{G_1}{2}\right)M_e\theta_w\xi\left(\frac{\partial C_{pe}}{\partial\theta}\right) \tag{62}$$

Integrating Eq. (62) gives the normal force and pitching moment derivatives at $\alpha=0$

$$\frac{\partial}{\partial\kappa}\left[\frac{d(\Delta c_{nd})}{d\theta}+\frac{d(\Delta c_{nc})}{d\theta}\right]\Big/\frac{dc_{ni}}{d\theta} = \frac{1}{2}\frac{\gamma(\gamma+2)}{\gamma+1}M_e\theta_w\left(1-\frac{G_1}{2}\right) \tag{63a}$$

$$\frac{\partial}{\partial\kappa}\left[\frac{d(\Delta c_{md})}{d\theta}+\frac{d(\Delta c_{mc})}{d\theta}\right]\Big/\frac{\partial}{\partial\kappa}\left[\frac{d(\Delta c_{nd})}{d\theta}+\frac{d(\Delta c_{nc})}{d\theta}\right] = -\left(\frac{2}{3}-\xi_{c.g.}\right) \tag{63b}$$

$$dc_{ni}/d\theta = 2(\partial C_{pe}/\partial\theta) \tag{63c}$$

Since there is no "piston cushioning" is this case, the total effect on the damping is the c_{mq} change. The equation corresponding to Eq. (19) is as follows:

$$\frac{d}{d\xi}\left\{\frac{\partial}{\partial\kappa}\left[\frac{d(\Delta c_{nd})}{d(cq/U_\infty)}+\frac{d(\Delta c_{nc})}{d(cq/U_\infty)}\right]\right\} = \frac{2\gamma(\gamma+2)}{\gamma+1}\left(1-\frac{G_1}{2}\right)M_e\theta_w\left(\frac{\partial C_{pe}}{\partial\theta}\right)\xi(\xi-\xi_{c.g.}) \tag{64}$$

Integration the moment contribution gives

$$\frac{\partial}{\partial\kappa}\left[\frac{d(\Delta c_{md})}{d(cq/U_\infty)}+\frac{d(\Delta c_{mc})}{d(cq/U_\infty)}\right]\Big/\frac{\partial}{\partial\kappa}\left[\frac{d(\Delta c_{nd})}{d(cq/U_\infty)}+\frac{d(\Delta c_{nc})}{d(cq/U_\infty)}\right] = -\left[\left(\frac{2}{3}-\xi_{c.g.}\right)^2+\frac{1}{18}\right] \tag{65}$$

In Fig. 13, the results from Eqs. (63) and (65) are shown for $M_\infty\ \theta_w=1.25$ and $M_e^2\gg 1$. Also shown are the predictions through Newtonian, Newtonian-Busemann, and Mandl's theories. The agreement between present prediction and Newtonian-Busemann theory is very good, which, of course, it should be for this case, i.e., for $M_\infty\to\infty$. The centrifugal pressure correction increases the Newtonian value by at most 20%. The figure shows that concave surface curvature increases the dynamic stability for all c.g. locations and increases the static stability for c.g. locations forward of $\xi_{c.g.}=\frac{2}{3}$. The effect of convex curvature is exactly the opposite. Whereas the agreement with experimental data has been found to be good for the Busemann correction to concave surface curvature effects,[32] no experimental verification for the convex curvature effects have been obtained.

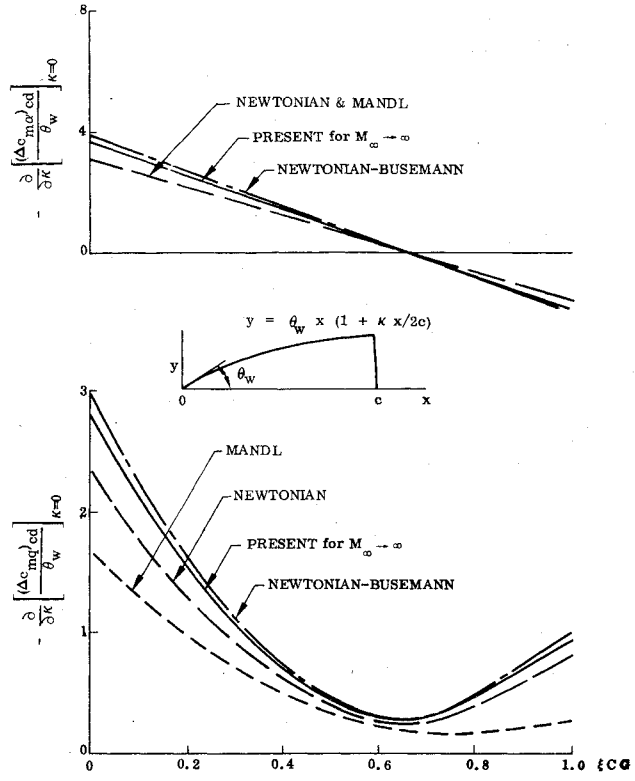

Fig. 13 Effect of longitudinal surface curvature and centrifugal pressure correction at $M_\infty\ \theta_w=1.25$.

Conclusions

A perturbation analysis of hypersonic unsteady aerodynamics has shown the following:

1 The results obtained by the developed viscous perturbation theory are in good agreement with those obtained using Orlik-Rückemann's numerical theory, and the theoretical predictions agree well with experimental results.

2. The predicted elastic deformation effects are in good agreement with available numerical results.

The presented analytic method should, because of its simplicity, make it possible to include viscous interaction effects in multi-degrees-of-freedom aeroelastic analyses.

Acknowledgment

The paper is based on results obtained in a study made for Dr. A. Somoroff and Dr. K. T. Yen, Naval Air Development Center, Warminister, Pa., under Contract N62269-73C-0713.

References

[1] Sliski, N. J., "An Analytical and Experimental Investigation of Hypersonic Viscous Interaction Pressure Effects," Air Force Flight Dynamics Laboratory, Wright-Patterson Air Force Base, AFFDL-TR-73-58, Nov. 1973.

[2] Orlik-Rückemann, K. J., "Dynamic Viscous Pressure-Interaction in Hypersonic-Flow," National Research Council of Canada, Aeronautical Rept. LR-535, July 1970.

[3] Orlik-Rückemann, K. J., "Oscillating Slender Cone in Viscous Hypersonic Flow," *AIAA Journal*, Vol. 10, Sept. 1972, pp. 1139-1140.

[4] Orlik-Rückemann, K. J. and LaBerge, J. G., "Oscillatory Experiments in a Helium Hypersonic Wind Tunnel," *Advances in Hypervelocity Techniques*, Plenum Press, New York, 1962, pp. 187-209.

[5] LaBerge, J. G. and Orlik-Rückemann, K. J., "Dynamic Stability Tests of Sharp Slender Wedges at $M=9$ and $M=18$ in Helium," National Aeronautical Establishment, Lab. Memo. No. HG 2-29, July 1968.

[6]Ericsson, L. E., "Unsteady Embedded Newtonian Flow," *Astronautica Acta*, Vol. 18, Nov. 1973, pp. 309-330.

[7]Ericsson, L. E., "Generalized Embedded Newtonian Flow," *Journal of Spacecraft and Rockets*, Vol. 12, Dec. 1975, pp. 718-726.

[8]Orlik-Rückemann, K. J., "Stability Derivatives of Sharp Wedges in Viscous Hypersonic Flow," *AIAA Journal*, Vol. 4, June 1966, pp. 1001-1007.

[9]Mandl, P., "Effect of Small Surface Curvature on Unsteady Hypersonic Flow Over an Oscillating Thin Wedge," *CASI Transactions*, Vol. 4, March 1971, pp. 47-57.

[10]Mandl, P., "Effect of Small Surface Curvature on Unsteady Hypersonic Flow Over an Oscillating Thin Wedge," Errata, *CASI Transactions*, Vol. 8, No. 2, 1975.

[11]Hayes, W. D. and Probstein, R. F., *Hypersonic Flow Theory*, Academic Press, New York and London, 1959.

[12]Bertram, M. H., "Hypersonic Laminar Viscous Interaction Effects on the Aerodynamics of Two-Dimensional Wedge and Triangular Planform Wings," NASA TND-3523, Aug. 1966.

[13]Yates, E. C. and Bennett, R. M., "Analysis of Supersonic-Hypersonic Flutter of Lifting Surfaces at Angle of Attack," *Journal of Aircraft*, Vol. 9, July 1972, pp. 481-489.

[14]Lighthill, J. J., "Oscillating Airfoils at High Mach Number," *Journal of Aerospace Sciences*, Vol. 20, June 1953, pp. 402-406.

[15]East, R. A., "A Theoretical and Experimental Study of Oscillating Wedge Shaped Airfoils in Hypersonic Flow," University of Southhampton, A.A.S.U. Rept. No. 228, Nov. 1962.

[16]VanDyke, M. D., "The Combined Supersonic-Hypersonic Similarity Rule," *Journal of Aerospace Sciences*, Vol. 18, July 1951, pp. 499-500.

[17]VanDyke, M. D., "Supersonic Flow Past Oscillating Airfoils Including Nonlinear Thickness Effects," NACA Rept. 1183, 1954.

[18]Hui, W. H., "Stability of Oscillating Wedges and Caret Wings in Hypersonic and Supersonic Flows," *AIAA Journal*, Vol. 7, Aug. 1969, pp. 1524-1530.

[19]Pugh, P. G. and Woodgate, L., "Measurements of Pitching-Moment Derivatives for Blunt-Nosed Aerofoils Oscillating in Two-Dimensional Supersonic Flow," Aeronautical Research Council, Great Britain, R&M No. 3315, July 1961.

[20]Scruton, C., Woodgate, L., Lapworth, K. C., and Maybrey, J., "Measurement of Pitching-Moment Derivatives for Aerofoils Oscillating in Two-Dimensional Supersonic Flow," Aeronautical Research Council, Great Britain, R&M No. 3234, Jan. 1959.

[21]Hulcher, G. D. and Behrens, W., "Viscous Hypersonic Flow over a Flat Plate at Angle of Attack with Leeside Boundary Layer Separation," *Proceedings of the 1972 Heat Transfer and Fluid Mechanics Institute*, Northridge, Calif., June 1972, pp. 108-127.

[22]Beastall, D. and Pallant, R. J., "Wind-Tunnel Tests on Two-Dimensional Supersonic Aerofoils at $M=1.86$ and $M=2.48$," Aeronautical Research Council, Great Britain, R&M No. 2800, July 1950.

[23]Ericsson, L. E., "Dynamic Effects of Shock-Induced Flow Separation," *Journal of Aircraft*, Vol. 12, Feb. 1975, pp. 86-92.

[24]Ericsson, L. E. and Reding, J. P., "Aerodynamic Effects of Bulbous Bases," NASA CR-1339, Aug. 1969.

[25]Ericsson, L. E. and Reding, J. P., "Re-entry Capsule Dynamics," *Journal of Spacecraft and Rockets*, Vol. 8, June 1971, pp. 575-586.

[26]Ericsson, L. E., "Supersonic Interference Flow Effects on Finned Bodies," *AIAA Journal*, Vol. 14, Sept. 1976, pp. 1342-1343.

[27]Ames Research Staff, "Equations, Tables, and Charts for Compressible Flow," NACA Rept. 1135, 1953.

[28]Schaaf, S. A., Moulic, E. S., Chahine, M. T., and Maslach, G. J., "Aerodynamic Characteristics of Wedges in Low Density Supersonic Flow," *ARS Journal*, Vol. 31, Feb. 1961, pp. 194-200.

[29]Tellep, D. M. and Talbot, L., "Normal Forces on Flat Plates in Low-Density Supersonic Flow," *Journal of the Aerospace Sciences*, Vol. 23, Dec. 1956, pp. 1099-1108.

[30]Bertram, M. H. and Blackstock, T. A., "Some Simple Solutions to the Problem of Predicting Boundary-Layer Self-Induced Pressures," NASA TND-798, April 1961.

[31]Ericsson, L. E., Almroth, B. O., Bailie, J. A., Brogan, F. A., and Stanley, G. M., "Hypersonic Aeroelastic Analysis," Contract N62269-73C-0713, Lockheed Missiles & Space Company, Inc., LMSC-D056746, Sept. 1975.

[32]Sullivan, P. A., "Inviscid Hypersonic Flow on Cusped Concave Surfaces," *Journal of Fluid Mechanics*, Vol. 24, Part 1, 1966, pp. 99-112.